



**HAL**  
open science

## Engineering the substrate and inhibitor specificities of human coagulation factor VIIa

Katrine S. Larsen, Henrik Østergaard, Jais R. Bjelke, Ole H. Olsen, Hanne B. Rasmussen, Leif Christensen, Birthe B. Kragelund, Henning R. Stennicke

► **To cite this version:**

Katrine S. Larsen, Henrik Østergaard, Jais R. Bjelke, Ole H. Olsen, Hanne B. Rasmussen, et al.. Engineering the substrate and inhibitor specificities of human coagulation factor VIIa. *Biochemical Journal*, 2007, 405 (3), pp.429-438. 10.1042/BJ20061901 . hal-00478727

**HAL Id: hal-00478727**

**<https://hal.science/hal-00478727>**

Submitted on 30 Apr 2010

**HAL** is a multi-disciplinary open access archive for the deposit and dissemination of scientific research documents, whether they are published or not. The documents may come from teaching and research institutions in France or abroad, or from public or private research centers.

L'archive ouverte pluridisciplinaire **HAL**, est destinée au dépôt et à la diffusion de documents scientifiques de niveau recherche, publiés ou non, émanant des établissements d'enseignement et de recherche français ou étrangers, des laboratoires publics ou privés.

## **Engineering the Substrate and Inhibitor Specificities of Human Coagulation Factor VIIa**

Katrine S. Larsen\*, Henrik Østergaard\*, Jais R. Bjelke<sup>†</sup>, Ole H. Olsen\*, Hanne B. Rasmussen<sup>†</sup>, Leif Christensen<sup>¶</sup>, Birthe B. Kragelund<sup>§</sup> and Henning R. Stennicke\*

\*Haemostasis Biochemistry, Novo Nordisk A/S, Novo Nordisk Park, DK-2760 Måløv, Denmark

<sup>†</sup>Protein Structure and Biophysics, Novo Nordisk A/S, Novo Nordisk Park, DK-2760 Måløv, Denmark

<sup>¶</sup>Biopharmaceutical Protein and Peptide Chemistry, Novo Nordisk A/S, Novo Nordisk Park, DK-2760 Måløv, Denmark

<sup>§</sup>Institute of Molecular Biology and Physiology, Structural Biology and NMR laboratory, University of Copenhagen, DK-1353 Copenhagen K, Denmark

**Running Title: Engineering Human Coagulation Factor VIIa**

**Keywords: Serpin, ATIII, specificity, profiling, protease, FVIIa**

**The atomic coordinates have been deposited in the Protein Data Bank, [www.rcsb.org](http://www.rcsb.org) (PDB ID 2PMM).**

## ABSTRACT

The remarkably high specificity of the coagulation proteases towards macromolecular substrates is provided by numerous interactions involving the catalytic groove and remote exosites. For factor VIIa (FVIIa), the principal initiator of coagulation via the extrinsic pathway, several exosites have been identified, whereas only little is known about the specificity dictated by the active-site architecture. Here, we have profiled the primary P4-P1 substrate specificity of FVIIa using positional scanning-substrate combinatorial libraries and evaluated the role of selective active site in defining specificity. Being a trypsin-like serine protease, FVIIa showed P1 specificity exclusively towards Arg and Lys. In the S2 pocket Thr, Leu, Phe and Val were the most preferred amino acids. Both S3 and S4 appeared to be rather promiscuous, however, with some preference for aromatic amino acids at both positions. Interestingly, a significant degree of interdependence between the S3 and S4 was observed, and as a consequence, the optimal substrate for FVIIa could not be derived directly from a sub-site directed specificity screen. To evaluate the role of the active site residues in defining specificity, a series of mutants of FVIIa were prepared at position 239 (c99), which is considered one of the most important residues for determining P2 specificity of the trypsin family members. This was confirmed for FVIIa by marked changes in primary substrate specificity and reduced rates of antithrombin III inhibition. Interestingly, these changes do not necessarily coincide with an altered ability to activate factor X demonstrating that inhibitor and macromolecular substrate selectivity may be engineered separately.

## Abbreviations

ACC, 7-amino-4-carbamoylmethylcoumarin; AMC, 7-amino-4methylcoumarin; APC, activated protein C; Arg152 (c15) etc, specific amino acid residues with chymotrypsin numbering in parentheses; ATIII, antithrombin III; BHK, baby hamster kidney cells; BSA, bovine serum albumin; cmk, chloromethyl ketone; ELISA, enzyme-linked immunosorbent assay; FVII, coagulation factor FVII; FVIIa, activated coagulation factor VII, FIX, coagulation factor IX; FIXa, activated coagulation factor IXa; FX, coagulation factor X; FXa, activated coagulation factor X; LMW, low molecular weight; MUGB, 4-methylumbelliferyl *p*-guanidinobenzoate; rFVIIa, recombinant activated coagulation factor VII; PS-SCL, positional scanning-substrate combinatorial library; serpin, serine protease inhibitor; sTF, soluble tissue factor (residues 1-219); T239I etc, substitution of Thr239 with Ile; TF, tissue factor; TFPI, tissue factor pathway inhibitor; tPA, tissue-type plasminogen activator. Nomenclature for the substrate amino acid preference is according to Schechter and Berger [1].

## INTRODUCTION

Coagulation factor VIIa (FVIIa) is a trypsin-like serine protease responsible for triggering blood coagulation when it associates with its cofactor tissue factor (TF) which is exposed upon vascular injury [2, 3]. TF-bound FVIIa is an efficient activator of both factor IX (FIX) and X (FX) which on the platelet surface ultimately results in a burst of thrombin, fibrin deposition, and the formation of a haemostatic plug [2]. Thus, initiation of blood coagulation represents a powerful and highly amplified system and for obvious reasons it must be tightly controlled in order to restrict thrombosis to the site of vessel injury and prevent complete occlusion of the damaged vessel. The enzymatic activity of FVIIa is regulated by two physiological inhibitors. The FVIIa-TF complex is efficiently inhibited by the Kunitz inhibitor tissue factor pathway inhibitor (TFPI) in the presence of FXa by forming an inhibitory TFPI-FXa-FVIIa-TF quaternary complex [4]. FVIIa can also be inhibited by the serine protease inhibitor (serpin) antithrombin III (ATIII) and the inhibition is accelerated many folds by sulphated glycosaminoglycans lining the vascular wall [5]. Interactions taking place at regions remote from the active site cleft, at so-called exosites, also influences the rate of TFPI inhibition of the FVIIa-TF complex and FXa [6], whereas the direct interaction between ATIII and its target proteases is mediated primarily through active site interactions and few exosite interactions [7].

From a molecular perspective, the interaction between FVIIa and TF is characterized by a large interface between their extracellular domains [8]. The activation of FIX and FX by this complex is mediated by extensive interactions involving both the Gla-EGF1 region and the protease domains of FIX and FX. Thus, the activation is largely considered to be controlled by exosite interactions remote from the active site [9, 10] and thus, ground state stabilization ( $K_m$ ) for the activation reaction may be largely independent of the active site. Consequently, we hypothesized that the inhibitory profile and the ability to act as an initiator of coagulation may constitute two independent paradigms in terms of substrate recognition. Thus, when altering substrate specificity there are a number of different strategies available among which the most obvious are: 1) blocking sites where large residues are preferred and 2) generating new cavities [11, 12]. Numerous attempts at engineering specific enzyme-substrate

interactions have been described in the literature; the general conclusion reached from these studies have been that major changes to substrate specificity often require global changes to the protein structure [13, 14]. In contrast to the challenge associated with generating new substrate specificities via the introduction of specific interactions, the generation of FVIIa variants that do not interact with ATIII, but maintain the ability to activate FX, appears to be of an entirely simpler nature.

In order to identify the most optimal sub-site for altering the FVIIa specificity we first evaluated the substrate specificity of FVIIa using positional scanning-substrate combinatorial libraries (PS-SCLs). One aspect that such libraries do not always fully address is the potential interdependence between the different sub-sites. Thus, in order to get a more detailed insight into the primary substrate selectivity of FVIIa we generated and analyzed a number of purified peptide substrates as well as generated a three dimensional structure of FVIIa-sTF in complex with a chloromethyl ketone (cmk) derivative mimicking an optimal substrate based on screening of the peptide substrates. Based on the findings from these studies a number of variants were generated by substituting residues within the active site cleft that form direct interactions with the side chains of the substrate [15, 16]. However, for reasons of simplicity only one position will be evaluated at present. From other trypsin family members such as tPA, FXa, APC and thrombin [16-18] position 99 (chymotrypsin numbering) has proven important for the S2 specificity of this family. Consequently, in order to reduce the rate of inhibition of FVIIa by circulating inhibitors while retaining proteolytic activity towards FX, we initially focused on this position in our attempts to alter the primary specificity of FVIIa.

## MATERIALS AND METHODS

*Materials*—Recombinant activated factor VIIa (rFVIIa) and soluble tissue factor (sTF, residues 1-219) was from Novo Nordisk A/S. Plasma-derived factor X (FX) and factor Xa (FXa) were from Enzyme Research Laboratories Ltd. Plasma-derived antithrombin III (ATIII) was from American Diagnostica inc. Low Molecular Weight (LMW) Heparin Sodium Salt from Porcine Intestinal Mucosa (molecular weight 5000 g/mol) was from Calbiochem. The chromogenic substrates S-2288 (D-Ile-Pro-Arg-p-nitroanilide) and S-2765 (benzyloxycarbonyl-D-Arg-Gly-Arg-p-nitroanilide) were from Chromogenix. The inhibitor Trp-Tyr-Thr-Arg-cmk was synthesized by SynPep. All oligonucleotides were from MWG-Biotech AG. All restriction endonucleases were from New England Biolabs. SDS-PAGE was run on 4-12% NuPAGE Novex Bis-Tris gels from Invitrogen. All other reagents were of analytical grade from Sigma-Aldrich.

*Mutagenesis and protein expression and purification*—The wild-type FVII expression plasmid pLN174 [19] was used as template for site directed mutagenesis using the QuikChange II XL Site-Directed Mutagenesis Kit (Stratagene). Plasmids were prepared using the QIAprep spin miniprep kit (QIAGEN) and the mutations were verified by DNA sequencing. Baby hamster kidney (BHK) cells were transfected with the FVII expression plasmids using the FuGENE6 Transfection Reagent (Roche) and the FVII variants purified as previously described [20]. After auto-activation the concentration of the FVIIa variants was determined by ELISA. All FVIIa variants were active site titrated with the ester substrate 4-methylumbelliferyl *p*-guanidinobenzoate (MUGB) essentially as described [21].

*Positional scanning-synthetic combinatorial libraries*—ACC-based PS-SCLs were synthesized at Novo Nordisk A/S by solid phase on Fmoc-7-amino-4-carbamoylmethylcoumarin resin essentially as previously described [20]. The four synthesized PS-SCLs consisted of 18 sub-libraries with each sub-library containing a mixture of tetrapeptide substrates incorporating one of the 18 proteinogenic amino acids (Met and Cys excluded) at P1, P2, P3 or P4. In the P2, P3 and P4 libraries Arg was fixed at P1 (preferred by FVIIa) and the last two positions were

randomized. In the P1 library the P1 residue was varied and the P2, P3 and P4 residues were all randomized. The concentration of the libraries was determined by amino acid analysis and absorbance measurements at 325 nm. The optimal emission and excitation parameters for assaying the PS-SCLs were determined by cleaving one of the P4 sub-libraries with trypsin. Each sub-library was assayed at final concentrations of 3, 6, 9 and 12  $\mu\text{M}$  in black 96-well fluorescence plates in a total reaction volume of 200  $\mu\text{l}$ . The assays were performed at room temperature in a buffer containing 50 mM Hepes, 100 mM NaCl, 5 mM  $\text{CaCl}_2$ , 0.01% Tween80, pH 7.4. The hydrolysis reactions were initiated by addition of a final concentration of 100 nM of FVIIa variant and 150 nM of sTF. Kinetics was monitored with a SpectraMax Gemini EM fluorescence microplate reader with excitation at 380 nm, emission at 455 nm and cutoff at 420 nm. The tetrapeptide substrates in each sub-library were assayed at a concentration far below the expected  $K_m$  and thus, linear fitting of the initial rates yielded a set of apparent second order rate constants for hydrolysis of each sub-library which were normalized to the rate of the sub-library with the highest activity.

*Assay of ACC-tetrapeptides*—23 ACC-tetrapeptides were synthesized on Fmoc-7-amino-4-carbamoylmethylcoumarin resin essentially as previously described [22]. The concentration of the peptides was determined by amino acid analysis and RP-HPLC. Each peptide was assayed in duplicate at final concentrations ranging from 0.78  $\mu\text{M}$  to 50  $\mu\text{M}$  in black 96-well fluorescence plates in a total reaction volume of 200  $\mu\text{l}$ . The assays were performed at room temperature in a buffer containing 50 mM Hepes, 100 mM NaCl, 5 mM  $\text{CaCl}_2$ , 0.01% Tween80, pH 7.4. The hydrolysis reactions were initiated by adding a final concentration of 10 nM of rFVIIa and 100 nM of sTF and kinetics was monitored using a SpectraMax Gemini EM fluorescence microplate reader with excitation at 380 nm, emission at 455 nm and cutoff at 420 nm.  $k_{\text{cat}}/K_m$  values were determined by linear fit of the data since  $[\text{S}]_0 \ll K_m$ .

*FVIIa activity assays*—All proteins were diluted in 50 mM Hepes, 100 mM NaCl, 5 mM  $\text{CaCl}_2$ , 1 mg/ml BSA, pH 7.4. The amidolytic activity was assayed with the chromogenic substrate S-

2288 (final concentrations 0.2-10 mM) in a total reaction volume of 200  $\mu$ l in 96-well plates. The reactions were initiated by addition of 10 nM of each FVIIa variant in the presence of 100 nM sTF. The absorbance increase was measured continuously at 405 nm in a SpectraMax 190 microplate reader.  $k_{\text{cat}}$  and  $K_{\text{m}}$  values were determined by fitting the data to the Michaelis-Menten equation by non-linear regression. When  $K_{\text{m}} > 5$  mM, only  $k_{\text{cat}}/K_{\text{m}}$  were determined by linear regression assuming  $[S]_0 \ll K_{\text{m}}$ .

The kinetic parameters of FX activation were determined by incubating 10 nM of each FVIIa variant with 100 nM of sTF and 0.1-6.4  $\mu$ M of FX (all final concentrations) for 20 minutes at room temperature in a total reaction volume of 100  $\mu$ l in 96-well plates. 50  $\mu$ l of stop buffer (50 mM HEPES, 100 mM NaCl, 20 mM EDTA, pH 7.4) was added followed by addition of 50  $\mu$ l of 2 mM substrate S-2765 and the absorbance increase was measured continuously at 405 nm in a SpectraMax 190 microplate reader. The  $k_{\text{cat}}/K_{\text{m}}$  values were determined and the amount of FXa generated was estimated from a standard curve generated with final concentrations of 0.5-10 nM active-site titrated FXa.

*Kinetics of ATIII inhibition*—The apparent second-order rate constant of inhibition,  $k_{\text{inh}}$ , was determined by the progress curve method monitoring competing hydrolytic and inhibition reactions [23]. All reagents were equilibrated at room temperature and the assay was performed in a buffer containing 50 mM HEPES, 100 mM NaCl, 5 mM  $\text{CaCl}_2$ , 1 mg/ml BSA, 0.1% PEG 8000, pH 7.4 in a total reaction volume of 200  $\mu$ l in 96-well plates. To maintain pseudo-first order conditions during the assay a minimum 10-fold excess of ATIII over FVIIa was used. In a 96-well plate 3  $\mu$ M LMW heparin was mixed with 50-750 nM ATIII. The reactions were started by adding 20  $\mu$ l of 2 mM S-2288 ensuring  $[S]_0 < K_{\text{m}}$  followed by addition of FVIIa and sTF to final concentrations of 5 and 50 nM, respectively. The absorbance increase was measured in a SpectraMax 190 microplate reader at 405 nm for 30 minutes to obtain progress curves at each inhibitor concentration.  $k_{\text{obs}}$  values were determined by fitting the progress curves to equation 1:

$$[\text{Pr}] = [\text{Pr}]_0 + \frac{v_0}{k_{\text{obs}}} (1 - e^{-k_{\text{obs}}t}) \quad (\text{Equation 1})$$

where  $[\text{Pr}]_0$  and  $[\text{Pr}]$  are the accumulation of product at assay start ( $t=0$ ) and at any time, respectively, visualized by a change in absorbance after addition of a chromogenic substrate.  $k_{\text{Lim}}$  and  $K_D$  values were obtained by fitting the  $k_{\text{obs}}$  values plotted against the inhibitor concentrations to a hyperbolic function which accounts for substrate binding (equation 2):

$$k_{\text{obs}} = \frac{k_{\text{Lim}}[\text{I}]_0}{K_D(1 + \frac{[\text{S}]_0}{K_m}) + [\text{I}]_0} \quad (\text{Equation 2})$$

where  $K_D$  is the dissociation constant for binding of FVIIa to the ATIII-heparin complex to form the non-covalent Michaelis-complex and  $k_{\text{Lim}}$  is the observed rate constant at saturation for formation of the covalent protease-inhibitor complex. The apparent second-order rate constant of inhibition,  $k_{\text{inh}}$ , is given by  $k_{\text{inh}} = k_{\text{Lim}}/K_D$ .

*FVIIa-ATIII complex breakdown*—Covalent complex breakdown was measured by making ATIII-FVIIa complexes at high concentrations of FVIIa and with ATIII in excess to ensure fast and complete inhibition. The reactions were then extensively diluted into a substrate-containing solution with  $[\text{S}]_0 \gg K_m$  and the restoration of protease activity was monitored continuously. The assay was performed in a buffer with 50 mM HEPES, 100 mM NaCl, 5 mM  $\text{CaCl}_2$ , 1 mg/ml BSA, 0.1% PEG 8000, pH 7.4. 0.5  $\mu\text{M}$  of rFVIIa was incubated with 2  $\mu\text{M}$  of sTF and 1.25 or 2.5  $\mu\text{M}$  of ATIII. A 4-fold excess of LMW heparin over ATIII was used. The reactions were incubated at room temperature for one hour. Each reaction was diluted 400, 450 and 500 times into 200  $\mu\text{l}$  reaction mixtures in a 96-well plate with a final concentration of 4 mM S-2288 and 100  $\mu\text{g/ml}$  of Polybrene. The absorbance increase at 405 nm was measured for 12 hours in a SpectraMax 190 microplate reader. The first-order rate constant of complex

breakdown,  $k_{\text{brkdn}}$ , was determined by fitting the absorbance curves to a single exponential function. The observed first-order rate constants were converted to half lives,  $t_{1/2}$ , according to the relationship  $t_{1/2} = \ln 2 / k_{\text{brkdn}}$ .

*Data analysis*—KaleidaGraph 3.6 from Synergy software or GraphPad Prism 4.0 was used to fit the data to the appropriate equations.

*Crystallization conditions*—The complex between WYTRcmk-FVIIa and sTF<sub>1-209</sub> was purified using a Superdex75 16/60 prep-grade column (Amersham Biosciences, Uppsala, Sweden) and concentrated to approximately 10 mg/ml using a Centriprep centrifugation device with a  $M_r$  cutoff of 50 kDa. A buffer composition of 10 mM Tris, 100 mM NaCl, 2 mM CaCl<sub>2</sub>, pH 7.5 was used. Crystal plates were obtained using the hanging drop vapor diffusion method using 0.1 M sodium citrate, 16.5-15.5 % (w/v) PEG4000, 12 % (v/v) 1-propanol, pH 5.6 as precipitating agent. A final protein concentration in the drop of approximately 3 mg/ml was used. Seeding was performed using crystal needles obtained as previously described [8].

*Crystal data collecting and processing*—Crystallographic data collection was performed at the Swiss Light Source synchrotron beam line PXI. Data reductions were performed with the XDS software package [24]. The structure was solved by the molecular replacement method using the MR facility of the CCP4 software package and the PDB entry 1DAN as a search model [25]. Model building was performed using Coot software [26] and iterative refinement (initially performed as a rigid body refinement) using RefMac5 of the CCP4 software package [25].

## RESULTS

*Specificity profiling of rFVIIa*—The positional scanning-substrate combinatorial libraries (PS-SCLs) were used to elucidate the substrate preference in the S1, S2, S3 and S4 binding pockets of rFVIIa. The libraries constitute a powerful tool for determination of protease specificity since a specificity profile for the individual sub-sites rapidly can be obtained by

monitoring the enzymatic liberation of the fluorogenic ACC. The PS-SCLs used in these studies were verified by amino acid analysis (data not shown) and the P1 library has previously been validated with three different proteases (trypsin, caspase-3 and subtilisin Carlsberg) showing the expected primary specificities [27]. Specificity profiling of rFVIIa in the presence of sTF showed as expected that rFVIIa only accepts Arg and Lys in the S1 pocket with Arg being favoured three times over Lys. In the S2 pocket  $\beta$ -branched or hydrophobic amino acids are allowed with Thr, Leu and Phe being the preferred residues (see Figure 1). In the S3 position the large aromatic residues Phe, Tyr and Trp are preferred, while the S4 sub-site appears highly promiscuous although a slight preference for Trp can be detected. An identical specificity profile of rFVIIa was obtained in the absence of sTF indicating that sTF do not alter the substrate specificity of rFVIIa (data not shown).

Assay of proteases with the PS-SCLs provides a complete specificity profile in the non-prime sites of the active site cleft. However, only one substrate-binding pocket is profiled at a time and therefore no steric considerations or interdependency between the sites are investigated. To elucidate any interdependency between the S1-S4 binding pockets, rFVIIa was assayed with a range of single ACC-tetrapeptides having Arg in P1; Thr or Leu in P2; Trp, Tyr, Leu or Ala in P3; and Trp, Phe or Asn in P4. The substrates were selected partly to address different levels of activity based on the specificity profiles and partly to explore the space around the natural FX cleavage site NLTR-IVGG. For technical reasons the NYTR-ACC peptide was omitted and thus rFVIIa was assayed with a total of 23 different ACC-tetrapeptides in the presence of sTF.

The obtained  $k_{cat}/K_m$  values for cleavage of the ACC-tetrapeptides by rFVIIa confirmed the preference for aromatic residues in both P3 and P4 (Table 1). The highest  $k_{cat}/K_m$  values were obtained for the WATR-ACC and WYTR-ACC peptides. The best peptide, WATR-ACC, was cleaved 3.6-fold more efficiently than the NLTR-ACC peptide, which represented the P4-P1 cleavage site in the activation peptide of FX. Peptides with P4-Asn were cleaved slowly compared to peptides with P4-Trp or P4-Phe except the NWTR-ACC peptide, which was cleaved with a rate similar to the WWTR-ACC and FWTR-ACC peptides probably due to the favourable

P3-Trp residue. For all peptides, rFVIIa was more active towards P2-Thr peptides than P2-Leu peptides by a factor of approximately 2.5. Thus, the clear P2-Thr specificity was independent of the nature of the P3 and P4 residue of the peptides.

The discrimination between two substrates is determined by the relative binding of their transition states to the enzyme. The difference in transition state stabilization energy,  $\Delta\Delta G_{\ddagger}^{\ddagger}$ , of the peptides was calculated using the relative difference in  $k_{\text{cat}}/K_{\text{m}}$  values [28] where  $\Delta\Delta G_{\ddagger}^{\ddagger}$  is negative if the XXXR peptide is a better substrate than the YYR peptide:

$$\Delta\Delta G_{\ddagger}^{\ddagger} = -RT \ln \frac{k_{\text{cat}}/K_{\text{m}}(\text{XXXR})}{k_{\text{cat}}/K_{\text{m}}(\text{YYR})}$$

Using this equation it was possible to evaluate the impact of a single substitution on the overall transition state stabilization energy as well as to assess whether there was interdependence between the different subsites. Interestingly, even with the relatively small number of substrates tested there appear to be quite a significant degree of interdependence as is evident from Figure 2. Thus, the effect on  $\Delta\Delta G_{\ddagger}^{\ddagger}$  of a single amino acid substitution is highly context dependent, e.g., in the extreme case the  $\Delta\Delta G_{\ddagger}^{\ddagger}$  for the P4 N->W substitution in the NATR-ACC peptide was  $-7.3 \text{ kJ} \cdot \text{mol}^{-1}$  while the same substitution in the NWTR-ACC peptide was only  $-0.4 \text{ kJ} \cdot \text{mol}^{-1}$ . For reference, in a system with no sub-site interdependence a  $\Delta\Delta G_{\ddagger}^{\ddagger}$  of  $-3.2 \text{ kJ} \cdot \text{mol}^{-1}$  would have been expected based on the sub-site profiling.

*Three dimensional structure of WYTRcmk-FVIIa in complex with sTF<sub>1-209</sub>*—To gain an increased insight into the manner in which an optimal substrate, as determined by the PS-SCL technique, binds to rFVIIa, the three dimensional structure of rFVIIa-sTF in complex with Trp-Tyr-Thr-Arg-chloromethyl ketone (cmk) was determined (Figure 3). The structure of the complex resolved to 2.05 Å based on 52,511 unique reflections observed giving 100 % completeness for the complete bin range 2.05 – 39.16 Å. Overall, the structure is highly similar to the structure of FVIIa-TF inhibited with Phe-Phe-Arg-cmk published by Banner et al [8]. The C $\alpha$

r.m.s.d. between the protease domain of the two structures is 0.3 Å. The covalently bound inhibitor was identified in the active site in the initial electron density map and build unbiased by excluding it during initial refinements. Interestingly, only the three first residues were clearly visible in the electron density map, *i.e.* Arg, Thr and Tyr (see Figure 3). Thus, to secure that the inhibitor was intact, the complex was analysed by MALDI-TOF MS, which demonstrated that the inhibitor had the expected sequence (data not shown).

The arginine in the P1 position was strongly defined and showed a similar binding motif as observed in the structure by Banner et al [6]. The P2 Thr residue is positioned adjunct to the catalytic triad with a distance of 3.4 Å to the catalytic His193 (c57), which also is the closest contact to any residue of the S2 pocket. The residue is within hydrogen bonding distance with the two water molecules W156 and W178 and could be part of a hydrogen-bonding network of the S2 pocket involving the para-positioned hydroxyl group of Tyr234 (c94), the carboxylate group of Asp196 (c60), the carbonyl of Thr238 (c98) and amides of both Gly237 (c97) and Thr238 (c98). No other contacts can be identified for the P2 residue.

The P3 Tyr residue interacts with the Gln313-Pro321 (c170-c170I) loop and the para-positioned hydroxyl group of the side chain of the tyrosine hydrogen bonds with the carbonyl of Asp319 (c170G), while the benzyl moiety interacts via hydrophobic contacts with Pro321 (c170I) and Trp364 (c215). The carbonyl of the Tyr hydrogen bonds with the amide of Gly367 (c216) as well as with water molecule W56 as earlier described. Thus, the observation that the preferred residue is Tyr, even compared to Phe and Trp, is reflected by the extra hydrogen bond donor of the side chain, which then leads to the more stabilized pocket as observed for the Gln313-Pro321 loop (c170-c170I).

*Expression and characterization of FVIIa variants*—A number of FVIIa variants modified in position 239 (c99) were generated to explore the effect of different side chain sizes. The variants were expressed in BHK cells and purified to homogeneity by a combination of anion exchange chromatography and immunoaffinity chromatography. After complete auto-activation, the FVIIa variants appeared as two bands on SDS-PAGE under reducing conditions

identical to wild-type FVIIa without visible signs of degradation (not shown). All FVIIa variants were active-site titrated with MUGB. The active site concentrations determined by the MUGB titrations were >75% relative to the concentrations determined by ELISA for all FVIIa variants except T239G.

*Enzymatic activity of FVIIa variants*—The enzymatic activity of the FVIIa variants towards small peptidyl substrates was analysed with the chromogenic peptide S-2288 (D-Ile-Pro-Arg-pNA) and the fluorogenic peptide WATR-ACC (Table 2). The amidolytic activity towards S-2288 was highly reduced for variants T239A, T239G and T239Y (4.8-, 10.9- and 10.8-fold, respectively, relative to wild-type rFVIIa). For variant T239I the  $k_{\text{cat}}/K_{\text{m}}$  values for cleavage of S-2288 was only slightly decreased compared to wild-type FVIIa. The amidolytic activity of all the FVIIa variants was improved when measured with the WATR-ACC peptide but the  $k_{\text{cat}}/K_{\text{m}}$  values were still lower compared to wild-type rFVIIa.

The FVIIa variants were analysed for their ability to activate FX in the presence of sTF (Table 2). The proteolytic activity was shown to be reduced 8-, 24- and 7-fold for variants T239A, T239G and T239Y, respectively, relative to wild-type rFVIIa whereas the  $k_{\text{cat}}/K_{\text{m}}$  value for activation of FX by variant T239I was comparable to that of wild-type rFVIIa.

*The influence of residue 239 (c99) on substrate specificity*—The effect of the introduced mutations on the substrate specificity was monitored with the PS-SCLs. Because of the limited amounts of purified FVIIa variants, T239A and T239G were only profiled with the P2 library whereas T239I and T239Y were profiled with both the P2 and P4 library. Phe, Thr and Leu were favourable P2 residues when Thr239 was substituted with either Ala or Gly but relative to wild-type rFVIIa the majority of the P2 sub-libraries were disfavoured. When Ile or Tyr was introduced in position 239 (c99) large changes in specificity were observed. T239I showed a 2.5- and 4-fold increased preference towards Trp and Tyr in P2, respectively, compared to wild-type rFVIIa. No changes in the P4 specificity were observed indicating that the introduced Ile residue was pointing into the S2 pocket and not influencing the specificity in the S4 pocket.

T239Y showed a 2.5-fold increased preference towards P2-Gly relative to wild-type rFVIIa. The P4 specificity was also affected by this mutation with all amino acids being nearly equally well tolerated as P4 residue and no clear preference for Trp was observed as seen in the P4 profile for wild-type rFVIIa. However, all the P4 sub-libraries were disfavoured for T239Y relative to wild-type rFVIIa.

*Kinetic parameters for ATIII inhibition of FVIIa variants*—The stoichiometry of inhibition (SI) for inhibition of wild-type rFVIIa and the FVIIa variants by ATIII in the presence of LMW heparin could not be determined accurately since the titration curves moved to higher  $[I]_0/[E]_0$  ratios as a function of time indicating breakdown of the ATIII-rFVIIa complexes (data not shown). The apparent second-order rate constant of inhibition ( $k_{inh}$ ) of wild-type rFVIIa and the FVIIa variants by ATIII was determined by the progress-curve method (Figure 5) with the results shown in Table 3. The wild-type rFVIIa-sTF complex was inhibited by ATIII in the presence of LMW heparin with an apparent second-order rate constant of inhibition of  $26917 \text{ M}^{-1} \cdot \text{s}^{-1}$ . Compared to wild-type rFVIIa, variants T239A and T239G were inhibited very slowly by ATIII with  $k_{inh}$  reduced 4.4- and 5.7-fold, respectively, reflecting their low enzymatic activities. In contrast, T239Y was inhibited slightly faster than wild-type rFVIIa. Interestingly, T239I showed a 40% reduction of  $k_{inh}$  relative to wild-type rFVIIa but maintained almost full activity against both S-2288 and FX.

*FVIIa-ATIII complex breakdown*—The first-order rate constant of covalent complex breakdown,  $k_{brkdn}$ , was determined for wild-type rFVIIa and the FVIIa variants by measuring the restoration of amidolytic activity over 12 hours of pre-formed serpin-protease complexes. Similar values of  $k_{brkdn}$  were obtained when the covalent complexes were made with 2.5- and 5-fold excess of ATIII relative to FVIIa confirming complete inhibition prior to measuring the complex breakdown. The obtained  $t_{1/2}$  for the complex of ATIII and wild-type rFVIIa was 5.6 hours (Table 3). The covalent complexes between ATIII and variants T239A, T239G and T239Y were more stable than the wild-type complex with  $t_{1/2}$  of 6.8, 12 and 9.3 hours,

respectively. In contrast, T239I formed an unstable complex with ATIII having  $t_{1/2}$  of 1.9 hours.

## DISCUSSION

The serine proteases of the haemostatic system are hallmarked by a marked and distinctive specificity towards endogenous substrates. This is required to tightly regulate the specific proteolytic events that convert inactive precursors in blood to active enzymes in the reactions leading to blood coagulation and fibrinolysis. FVIIa plays a crucial role in the haemostatic system by initiating blood coagulation upon vascular injury. In the current study the substrate and inhibitor specificity of FVIIa has been evaluated using small peptidyl substrates, physiological macromolecular substrates as well as site-directed mutagenesis of key residues in the active site cleft of FVIIa. As expected, rFVIIa only accepted positively charged amino acids in the S1 pocket with a 3-fold higher preference towards Arg relative to Lys. In the P2 position hydrophobic or  $\beta$ -branched amino acids were favoured (Thr>Leu>Phe>Val) and aromatic amino acids were preferred in the S3 pocket. Thus, the specificity profile clearly demonstrates that rFVIIa is not a very discriminative protease with low degree of active site specificity. The selectivity index defined by the ratio between the apparent second order rate constant of the best and worst sub-library is 26 in the P2 specificity profile of rFVIIa. Thus, the P2 selectivity for rFVIIa appears to be more like trypsin, which has a selectivity index of 12, than FXa or thrombin which are characterized by selectivity indexes of 290 and 19000, respectively [29]. Recently, the P2 and P3 specificity of FVIIa has been profiled using fluorogenic peptide micro-arrays [30]. In that study Thr and Val were also found to be favourable P2 residues, however, in P3 the investigators found Gln, Arg, Asn and Pro to be preferred, in contrast to the preference towards aromatic amino acids found in the current study. The basis for this difference remains unclear, however, it may be due to a possible interdependence between S3 and S4 as the study by Gosalia et al utilizes Ala in P4 [30] and the present study uses a degenerated pool of amino acids.

In the P4 position there was a pronounced preference towards Trp which is in agreement with a study searching for extensions to the A-183 peptide [31], where it was found by Maun et al that the best sequence extending into the active site of rFVIIa also had a Trp in P4. From modelling studies, the P4 Trp was expected to make favourable  $\pi$ - $\pi$  interactions with Trp364 (c215) in the bottom of the putative S4 pocket. However, to our surprise the structure of the WYTRcmk-FVIIa-sTF complex showed no electron density corresponding to the P4 Trp (see Figure 3) indicating that there is not a well-defined S4 pocket in FVIIa despite the clear preference observed within the libraries. This could be explained by suboptimal interactions between the P4 residue and the S4 pocket, which would result in a poorly defined electron density because of high temperature factors and suggest that FVIIa may not have a well-defined S4 sub-site. This notion is to some extent supported by the structure as well as the fact that the natural substrate for FVIIa is the N\*LTR-IVGG site of FX which harbours a glycosylated Asn in the P4 position.

A review of a large number of proteases in the PDB database has revealed that proteases generally bind their substrates in an extended binding conformation which is to a large degree defined by  $\beta$ -strand type backbone interactions [32, 33]. The PS-SCLs profile the primary selectivity in the S1-S4 binding pockets of a protease independently without accounting for cross-talk between sub-sites and without the requirements for optimal alignment of the peptide backbone. To address this issue, interdependency between the S1-S4 binding sites of rFVIIa was investigated by determining the change in transition state stabilization energy,  $\Delta\Delta G_T^\ddagger$ , upon a single substitution in the substrate, e.g., WATR-ACC to FATR-ACC etc. As demonstrated by the derived data accumulated in Figure 2, there is a significant degree of interdependence between the different sub-sites as indicated by the relatively large differences associated with identical amino acid substitutions in different scaffolds, i.e., the  $\Delta\Delta G_T^\ddagger$  for a P4 substitution of Asn  $\rightarrow$  Trp or Phe is very different for substrates with different P3 residues, while only minor differences are observed between similar substrates with Leu or Thr in P2. Thus, the S3 selectivity is likely to be driven or influenced by the P4 occupancy and this could

potentially explain the difference between the two rather similar approaches used to describe FVIIa specificity.

Interestingly, the effects of going from Asn in P4 of NATR-ACC to Phe or Trp far exceeds the predicted effects from the sub-site profiling as  $\Delta\Delta G_T^\ddagger$  values of -1.4 and -3.1 kJ · mol<sup>-1</sup>, respectively, were expected rather than the observed -5 and -7 kJ · mol<sup>-1</sup>, respectively. This is in contrast to the changes observed for the Phe to Trp substitution, which are very close to what should be anticipated from the profiling. One explanation for this observation is that optimal sub-site occupancy does not translate to one optimal substrate. As a result, if P3 contains Trp or Phe the influence of P4 is ablated in agreement with the observation that no electron density is visible for the P4 Trp in the X-ray structure of the WYTRcmk-FVIIa-sTF complex. Consequently, the effect of substituting Asn for a large aromatic amino acid in P4 will be underestimated in the PS-SCLs due to the requirement for a suboptimal P3 substituent for efficient catalysis.

Since the predominating specificity of FVIIa appears to be located to S1 and S2 we examined the S2 binding site for residues that may alter the substrate recognition. Thr239 (c99) is localized at the interface between the S2 and S4 binding pocket in the active site cleft and could potentially influence the substrate specificity in these binding pockets (see Figure 3). The effect of substituting Thr239 with Ala, Gly, Ile and Tyr, respectively, was evaluated. All variants showed very low amidolytic and proteolytic activity relative to wild-type rFVIIa except variant T239I, which had an activity comparable to wild-type rFVIIa. Thus, just like FIXa [34], FVIIa is highly sensitive to mutations in this position indicating that it is important in the substrate and inhibitor recognition by FVIIa.

Substitution of Thr239 with Tyr caused a 2.5-fold increased preference towards P2 Gly and a broader P4 specificity profile compared to wild-type rFVIIa. Interestingly, despite the very low catalytic activity of T239Y, this variant was inhibited by ATIII at a rate comparable to wild-type

rFVIIa. This is presumably due to the observed P2 Gly specificity of T239Y as ATIII has Gly in the P2 position of the reactive center loop. This is in accordance with FXa having Tyr in this position also showing a P2 preference towards Gly and being rapidly inhibited by ATIII, which indicated that the T239Y mutation in FVIIa transmitted a FXa-like P2 specificity. The increased propensity of P2 Gly specific proteases to inhibition by ATIII has also been demonstrated with gla-domainless APC T254Y (c99) showing an increased preference towards chromogenic substrates with P2-Gly residues and a 181-fold more efficient inhibition by ATIII compared to gla-domainless APC [16].

Substitution of Thr239 in FVIIa with Ile resulted in a 40% decrease in the apparent second-order rate constant of inhibition by ATIII relative to wild-type rFVIIa indicating an important role of residue 239 in the interaction with ATIII. Interestingly, the T239I mutation did not affect the proteolytic activity towards FX markedly. The general importance of residue c99 on the rate of inhibition by ATIII has been demonstrated with the thrombin variants L281Y, L281T and L281G (c99) where the apparent second-order rate constant was decreased 2-, 42- and 65-fold, respectively, indicating that the larger hydrophilic S2 pockets of FVIIa and APC are not optimal for interacting with ATIII [16]. T239I favoured large aromatic P2 residues revealed by a 2.5- and 4-fold increased preference towards P2 Trp and P2 Tyr, respectively, relative to wild-type rFVIIa. However, T239I also showed a slightly increased P2 Gly preference (1.5-fold) but was inhibited slower by ATIII compared to T239Y and wild-type rFVIIa thus indicating that the inhibition of FVIIa by ATIII might be more complex. These findings nicely support the notion derived from the structure, which indicates that the preference for Thr is not associated with specific residue interactions.

Recent studies of FXa have demonstrated that the P2 Gly preference does not solely determine the specificity towards ATIII indicated by the findings that interactions at secondary sites outside the P6-P3' region also influence the inhibition of FXa by ATIII [35]. In addition, an exosite within strand 3 of  $\beta$ -sheet C of ATIII has been identified and shown to be important in the reaction of ATIII with FIXa and FXa [36].

The importance of residues within the putative S2 pocket of proteases to the inhibition by serpins has been confirmed by a mutagenesis study of APC [37]. Substitution of residues within the active site cleft of APC resulted in variants exhibiting resistance to inhibition by protein C inhibitor and  $\alpha_1$ -antitrypsin yet maintained anticoagulant activity. When Thr254 (c99) was substituted with Ser the half-life in human plasma was prolonged 2-fold due to reduced rates of inactivation by circulating serpins found in plasma. The effect was more pronounced when the T254S (c99) mutation was combined with mutations of residue Leu194 (c40) yielding up to 11-fold prolongation of the plasma half-life [37]. Thus, it appears that residue c99 in homologous enzymes as FVIIa and APC influences the inhibitor specificity towards different serpins.

This study of FVIIa and the APC variants described by Berg et al. [37] shows how it is possible to engineer the primary specificity of serine proteases without compromising their biological function in the propagation and regulation of the coagulation cascade. These interesting findings reinforce the notion that the *in vivo* specificity of proteases towards their macromolecular substrates is to a large degree dictated by exosite interactions. As a result, it is clearly possible to separately engineer the recognition of macromolecular substrates and inhibitors. Thus, by substituting key residues in the active site cleft of FVIIa the specificity towards peptidyl substrates as well as towards physiological inhibitors, e.g. ATIII, can be altered thereby influencing the rate of inactivation without significantly altering the ability to activate FX.

## REFERENCES

- 1 Schechter, I. and Berger, A. (1967) On the size of the active site in proteases. I. Papain. *Biochem. Biophys. Res. Commun.* **27**, 157-62
- 2 Davie, E. W., Fujikawa, K. and Kisiel, W. (1991) The coagulation cascade: initiation, maintenance, and regulation. *Biochemistry* **30**, 10363-70
- 3 Perona, J. J. and Craik, C. S. (1995) Structural basis of substrate specificity in the serine proteases. *Protein Sci.* **4**, 337-60
- 4 Broze, G. J., Jr., Warren, L. A., Novotny, W. F., Higuchi, D. A., Girard, J. J. and Miletich, J. P. (1988) The lipoprotein-associated coagulation inhibitor that inhibits the factor VII-

- tissue factor complex also inhibits factor Xa: insight into its possible mechanism of action. *Blood* **71**, 335-43
- 5 Olson, S. T., Bjork, I., Sheffer, R., Craig, P. A., Shore, J. D. and Choay, J. (1992) Role of the antithrombin-binding pentasaccharide in heparin acceleration of antithrombin-proteinase reactions. Resolution of the antithrombin conformational change contribution to heparin rate enhancement. *J. Biol. Chem.* **267**, 12528-38
- 6 Petersen, L. C., Bjorn, S. E., Olsen, O. H., Nordfang, O., Norris, F. and Norris, K. (1996) Inhibitory properties of separate recombinant Kunitz-type-protease-inhibitor domains from tissue-factor-pathway inhibitor. *Eur. J. Biochem.* **235**, 310-6
- 7 Chuang, Y. J., Swanson, R., Raja, S. M., Bock, S. C. and Olson, S. T. (2001) The antithrombin P1 residue is important for target proteinase specificity but not for heparin activation of the serpin. Characterization of P1 antithrombin variants with altered proteinase specificity but normal heparin activation. *Biochemistry* **40**, 6670-9
- 8 Banner, D. W., D'Arcy, A., Chene, C., Winkler, F. K., Guha, A., Konigsberg, W. H., Nemerson, Y. and Kirchhofer, D. (1996) The crystal structure of the complex of blood coagulation factor VIIa with soluble tissue factor. *Nature* **380**, 41-6
- 9 Shobe, J., Dickinson, C. D., Edgington, T. S. and Ruf, W. (1999) Macromolecular substrate affinity for the tissue factor-factor VIIa complex is independent of scissile bond docking. *J. Biol. Chem.* **274**, 24171-5
- 10 Baugh, R. J., Dickinson, C. D., Ruf, W. and Krishnaswamy, S. (2000) Exosite interactions determine the affinity of factor X for the extrinsic Xase complex. *J. Biol. Chem.* **275**, 28826-33
- 11 Bone, R., Silen, J. L. and Agard, D. A. (1989) Structural plasticity broadens the specificity of an engineered protease. *Nature* **339**, 191-5
- 12 Bone, R., Sampson, N. S., Bartlett, P. A. and Agard, D. A. (1991) Crystal structures of alpha-lytic protease complexes with irreversibly bound phosphonate esters. *Biochemistry* **30**, 2263-72
- 13 Hedstrom, L. (2002) Serine protease mechanism and specificity. *Chem. Rev.* **102**, 4501-24
- 14 Hedstrom, L., Szilagyi, L. and Rutter, W. J. (1992) Converting trypsin to chymotrypsin: the role of surface loops. *Science* **255**, 1249-53
- 15 Chang, Y. J., Hamaguchi, N., Chang, S. C., Ruf, W., Shen, M. C. and Lin, S. W. (1999) Engineered recombinant factor VII Q217 variants with altered inhibitor specificities. *Biochemistry* **38**, 10940-8
- 16 Rezaie, A. R. (1996) Role of residue 99 at the S2 subsite of factor Xa and activated protein C in enzyme specificity. *J. Biol. Chem.* **271**, 23807-14
- 17 Vindigni, A., Winfield, M., Ayala, Y. and Di Cera, E. (2000) Role of residue Y99 in tissue plasminogen activator. *Protein Sci.* **9**, 619-622
- 18 Rezaie, A. R. (1997) Role of Leu99 of thrombin in determining the P2 specificity of serpins. *Biochemistry* **36**, 7437-46
- 19 Persson, E. and Nielsen, L. S. (1996) Site-directed mutagenesis but not gamma-carboxylation of Glu-35 in factor VIIa affects the association with tissue factor. *FEBS Lett.* **385**, 241-3
- 20 Persson, E., Nielsen, L. S. and Olsen, O. H. (2001) Substitution of aspartic acid for methionine-306 in factor VIIa abolishes the allosteric linkage between the active site and the binding interface with tissue factor. *Biochemistry* **40**, 3251-6
- 21 Payne, M. A., Neuenschwander, P. F., Johnson, A. E. and Morrissey, J. H. (1996) Effect of soluble tissue factor on the kinetic mechanism of factor VIIa: enhancement of p-guanidinobenzoate substrate hydrolysis. *Biochemistry* **35**, 7100-6
- 22 Maly, D. J., Leonetti, F., Backes, B. J., Dauber, D. S., Harris, J. L., Craik, C. S. and Ellman, J. A. (2002) Expedient solid-phase synthesis of fluorogenic protease substrates using the 7-amino-4-carbamoylmethylcoumarin (ACC) fluorophore. *J. Org. Chem.* **67**, 910-5
- 23 Schechter, N. M. and Plotnick, M. I. (2004) Measurement of the kinetic parameters mediating protease-serpin inhibition. *Methods* **32**, 159-68

- 24 Kabsch, W. (1993) Automatic processing of rotation diffraction data from crystals of  
initially unknown symmetry and cell constants. *J. Appl. Cryst.* **26**, 795-800
- 25 Potterton, E., Briggs, P., Turkenburg, M. and Dodson, E. (2003) A graphical user  
interface to the CCP4 program suite. *Acta Crystallogr D Biol Crystallogr* **59**, 1131-7
- 26 Emsley, P. and Cowtan, K. (2004) Coot: model-building tools for molecular graphics.  
*Acta. Crystallogr. D. Biol. Crystallogr.* **60**, 2126-32
- 27 Snipas, S. J., Wildfang, E., Nazif, T., Christensen, L., Boatright, K. M., Bogoy, M.,  
Stennicke, H. R. and Salvesen, G. S. (2004) Characteristics of the caspase-like catalytic  
domain of human paracaspase. *Biol. Chem.* **385**, 1093-8
- 28 Gron, H., Meldal, M. and Breddam, K. (1992) Extensive comparison of the substrate  
preferences of two subtilisins as determined with peptide substrates which are based on  
the principle of intramolecular quenching. *Biochemistry* **31**, 6011-8
- 29 Bianchini, E. P., Louvain, V. B., Marque, P. E., Juliano, M. A., Juliano, L. and Le Bonniec,  
B. F. (2002) Mapping of the catalytic groove preferences of factor Xa reveals an  
inadequate selectivity for its macromolecule substrates. *J. Biol. Chem.* **277**, 20527-34
- 30 Gosalia, D. N., Salisbury, C. M., Ellman, J. A. and Diamond, S. L. (2005) High  
throughput substrate specificity profiling of serine and cysteine proteases using  
solution-phase fluorogenic peptide microarrays. *Mol. Cell. Proteomics* **4**, 626-36
- 31 Maun, H. R., Eigenbrot, C. and Lazarus, R. A. (2003) Engineering exosite peptides for  
complete inhibition of factor VIIa using a protease switch with substrate phage. *J. Biol.  
Chem.* **278**, 21823-30
- 32 Tyndall, J. D. and Fairlie, D. P. (1999) Conformational homogeneity in molecular  
recognition by proteolytic enzymes. *J. Mol. Recognit.* **12**, 363-70
- 33 Tyndall, J. D., Nall, T. and Fairlie, D. P. (2005) Proteases universally recognize beta  
strands in their active sites. *Chem. Rev.* **105**, 973-99
- 34 Sichler, K., Kopetzki, E., Huber, R., Bode, W., Hopfner, K. P. and Brandstetter, H.  
(2003) Physiological fIXa activation involves a cooperative conformational  
rearrangement of the 99-loop. *J. Biol. Chem.* **278**, 4121-6
- 35 Chuang, Y. J., Swanson, R., Raja, S. M. and Olson, S. T. (2001) Heparin enhances the  
specificity of antithrombin for thrombin and factor Xa independent of the reactive center  
loop sequence. Evidence for an exosite determinant of factor Xa specificity in heparin-  
activated antithrombin. *J. Biol. Chem.* **276**, 14961-71
- 36 Izaguirre, G., Zhang, W., Swanson, R., Bedsted, T. and Olson, S. T. (2003) Localization  
of an antithrombin exosite that promotes rapid inhibition of factors Xa and IXa  
dependent on heparin activation of the serpin. *J. Biol. Chem.* **278**, 51433-40
- 37 Berg, D. T., Gerlitz, B., Shang, J., Smith, T., Santa, P., Richardson, M. A., Kurz, K. D.,  
Grinnell, B. W., Mace, K. and Jones, B. E. (2003) Engineering the proteolytic specificity  
of activated protein C improves its pharmacological properties. *Proc. Natl. Acad. Sci.*  
**100**, 4423-8

## LEGENDS

**Table 1.**  $k_{\text{cat}}/K_{\text{m}}$  values ( $\text{mM}^{-1} \cdot \text{s}^{-1}$ ) for cleavage of ACC-tetrapeptides of the format P4-P3-P2-Arg-ACC by rFVIIa in the presence of sTF measured in 50 mM Hepes, 100 mM NaCl, 5 mM  $\text{CaCl}_2$ , 0.01% Tween80, pH 7.4. n.d., not determined.

**Table 2.**  $k_{\text{cat}}/K_{\text{m}}$  values for cleavage of S-2288 and WATR-ACC as well as activation of FX by rFVIIa and the FVIIa variants in the presence of sTF measured in 50 mM Hepes, 100 mM NaCl, 5 mM  $\text{CaCl}_2$ , 1 mg/ml BSA, pH 7.4.

**Table 3.** The apparent second-order rate constants for inhibition,  $k_{\text{inh}}$ , of the FVIIa variants by ATIII determined as the ratio  $k_{\text{inh}}=k_{\text{Lim}}/K_{\text{D}}$  measured in the presence of sTF and LMW heparin in 50 mM Hepes, 100 mM NaCl, 5 mM  $\text{CaCl}_2$ , 1 mg/ml BSA, 0.1% PEG8000, pH 7.4. The first-order rate constants of complex breakdown,  $k_{\text{brkdn}}$ , and  $t_{1/2}$  determined as the average of six independent measurements.  $t_{1/2}$  was calculated by the relation  $t_{1/2}=\ln 2/k_{\text{brkdn}}$ .

**Figure 1.** Specificity profile of rFVIIa in the presence of sTF measured in 50 mM Hepes, 100 mM NaCl, 5 mM  $\text{CaCl}_2$ , 0.01% Tween80, pH 7.4. In each library the apparent second-order rate constants of substrate hydrolysis were normalized to the sub-library with the highest activity. Full line: Mean value of all the columns. Dotted line: 1× standard deviation of all the columns.

**Figure 2.** Interdependence of FVIIa sub-sites as illustrated by the changes in transition state stabilization energies ( $\Delta\Delta G^\ddagger$  values) for cleavage of ACC-tetrapeptides (P4-P3-P2-Arg-ACC) for the substitution of P4 N->W (solid), N->F (empty) and F->W (hatched) as a function of the P3 residues with P2 = L (left panel) and P2 = T (right panel). The pred column reflects

the  $\Delta\Delta G^\ddagger$  value anticipated based on the sub-site profiling. As it is evident there is significant impact of P3 on the substitution of P4 residues, but only minor influence of P2.

**Figure 3.** Crystal structure of WYTRcmk-FVIIa-sTF<sub>1-209</sub> obtained at 2.05 Å resolution. Figure A is shown in standard orientation. The orientation of figure B and C is slightly changed for optimal view. A) View of the protease domain in an electro-potential surface plot with the inhibitor shown with a  $2F_oF_c$  electron density map with  $2\sigma$  cut-off (Colour scales: negative charges red, positive charges blue, carbon grey, oxygen red and nitrogen blue). The S1, S2 and S3 pockets are indicated with arrows. Note the striking difference between S1 and S2 compared to S3 in which the formers are distinct cavities with defined boundaries and high degree of electro-negativity, while the S3 pocket is flat with an almost neutral electro-potential surface. No obvious S4 pocket can be identified surrounding the active site in accordance with the lack of electron density for the P4 residue. B) Close-up of selected residues within a 5 Å sphere of the covalently bound inhibitor shown with a  $2F_oF_c$  electron density map with  $2\sigma$  cut-off. As indicated, the electron density traced the active site residues well. Carbons of the inhibitor are coloured orange to distinguish it from protein carbons. C) Highlight of specific interactions of the selected active site residues and covalently bound inhibitor (view is slightly tilted compared to B). The S1, S2 and S3 composition is shown with brackets and residue identifications are given with chymotrypsin numbering. Hydrogen bonding networks are shown in orange dotted lines. The following secondary elements are coloured accordingly: Lys336 – Gly346 blue, His373 – Tyr377 green, Val362 – Ala369 yellow and Gln313 – Asn322 raspberry red. See main text for details.

**Figure 4.** Specificity profiles of FVIIa variants modified in position 239 measured in the presence of sTF in 50 mM Hepes, 100 mM NaCl, 5 mM CaCl<sub>2</sub>, 0.01% Tween80, pH 7.4. The columns in grey show the apparent second-order rate constants of substrate hydrolysis ( $M^{-1} \cdot s^{-1}$ )

<sup>1</sup>) of each sub-library. The columns in black show the apparent second-order rate constants of substrate hydrolysis relative to wt rFVIIa for each sub-library. wt, wild-type.

**Figure 5.** The rate of inhibition of rFVIIa and the FVIIa variants by ATIII was determined by the progress-curve method under pseudo-first order conditions measured in the presence of sTF and LMW heparin in 50 mM Hepes, 100 mM NaCl, 5 mM CaCl<sub>2</sub>, 1 mg/ml BSA, 0.1% PEG8000, pH 7.4.  $k_{\text{Lim}}$  and  $K_{\text{D}}$  values were determined by plotting the  $k_{\text{obs}}$  values against the concentration of ATIII and fitting the data to equation 2 (in Materials and Methods). The apparent second-order rate constant of inhibition,  $k_{\text{inh}}$ , was determined as the ratio  $k_{\text{inh}} = k_{\text{Lim}}/K_{\text{D}}$ . ●, rFVIIa; ■, T239A; ◆, T239G; ▲, T239I; ▼, T239Y.

Table 1.

| <b>P2 = T</b> |          | <b>P3</b>  |            |            |            |
|---------------|----------|------------|------------|------------|------------|
|               |          | <b>A</b>   | <b>L</b>   | <b>Y</b>   | <b>W</b>   |
| <b>P4</b>     | <b>N</b> | 2.6 ± 0.04 | 13.8 ± 0.1 | n.d.       | 19.6 ± 0.4 |
|               | <b>F</b> | 19.4 ± 0.5 | 12.2 ± 0.5 | 24.5 ± 0.2 | 24.6 ± 0.3 |
|               | <b>W</b> | 49.8 ± 0.6 | 25.8 ± 0.3 | 44.0 ± 0.4 | 23.7 ± 0.2 |

| <b>P2 = L</b> |          | <b>P3</b>   |             |             |            |
|---------------|----------|-------------|-------------|-------------|------------|
|               |          | <b>A</b>    | <b>L</b>    | <b>Y</b>    | <b>W</b>   |
| <b>P4</b>     | <b>N</b> | 1.1 ± 0.005 | 5.7 ± 0.07  | 9.8 ± 0.04  | 11.2 ± 0.1 |
|               | <b>F</b> | 9.7 ± 0.1   | 7.8 ± 0.2   | 7.4 ± 0.1   | 7.2 ± 0.2  |
|               | <b>W</b> | 19.2 ± 0.3  | 11.7 ± 0.08 | 18.0 ± 0.08 | 6.1 ± 0.04 |

Table 2.

|            | $k_{cat}/K_m$<br>(mM <sup>-1</sup> · s <sup>-1</sup> ) |                 |           |
|------------|--|-----------------|-----------|
|            | <b>S-2288</b>  | <b>WATR-ACC</b> | <b>FX</b> |
| rFVIIa-sTF | 26.12 ± 2.77   | 44.66 ± 0.11    | 550 ± 30  |
| T239A-sTF  | 5.45 ± 0.15  | 28.59 ± 0.08    | 69 ± 5    |
| T239G-sTF  | 2.40 ± 0.036   | 17.59 ± 0.10    | 23 ± 0.6  |
| T239I-sTF  | 19.71 ± 2.26   | 29.01 ± 0.07    | 461 ± 12  |
| T239Y-sTF  | 2.47 ± 0.18  | 6.08 ± 0.02     | 74 ± 5    |

**Table 3.**

|        | $k_{\text{Lim}}$<br>( $10^{-3} \text{ s}^{-1}$ ) | $K_{\text{D}}$<br>( $10^{-7} \text{ M}$ ) | $k_{\text{inh}}$<br>( $\text{M}^{-1} \cdot \text{s}^{-1}$ ) | $k_{\text{brkdn}}$<br>( $10^{-5} \text{ s}^{-1}$ ) | $t_{1/2}$<br>(hours) |
|--------|--|---|---|--|----------------------|
| rFVIIa | 4.9 ± 0.32                                       | 1.81 ± 0.33                               | 26917 ± 5237  | 3.43   | 5.6                  |
| T239A  | 1.6 ± 0.10                                       | 2.60 ± 0.41                               | 6160 ± 1058   | 2.85   | 6.8                  |
| T239G  | 1.5 ± 0.14                                       | 1.14 ± 0.71                               | 4688 ± 1155   | 1.61   | 12.0                 |
| T239I  | 2.4 ± 0.12                                       | 1.45 ± 0.22                               | 16338 ± 2564  | 10.20  | 1.9                  |
| T239Y  | 5.3 ± 0.29                                       | 1.74 ± 0.26                               | 30591 ± 4906  | 2.08   | 9.3                  |

Figure 1.

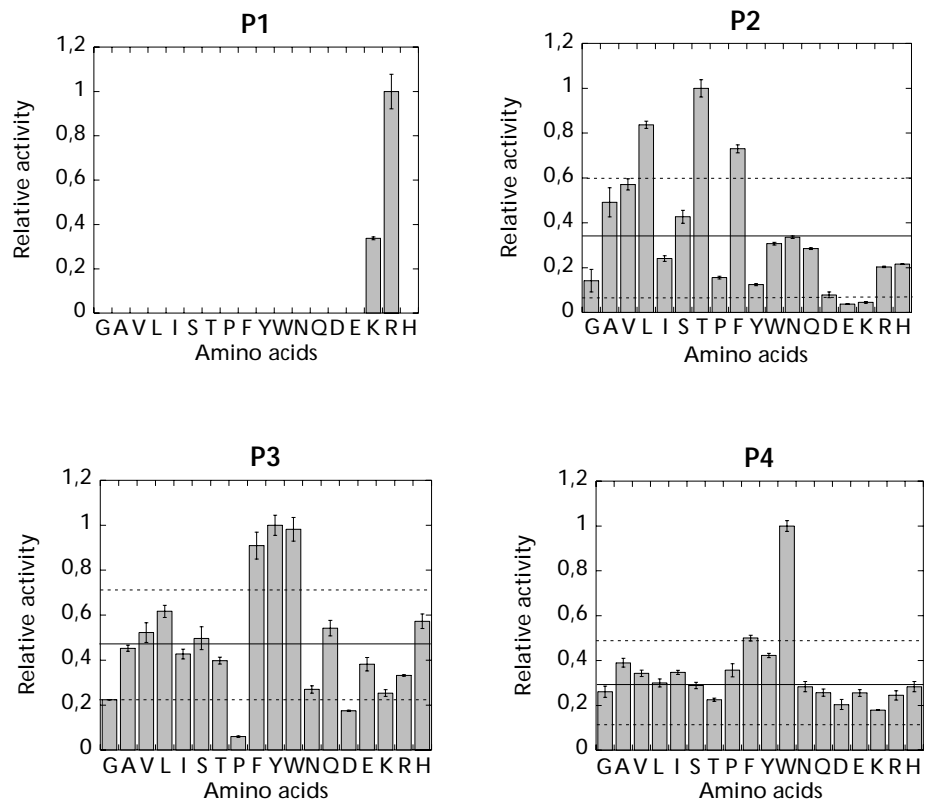


Figure 2.

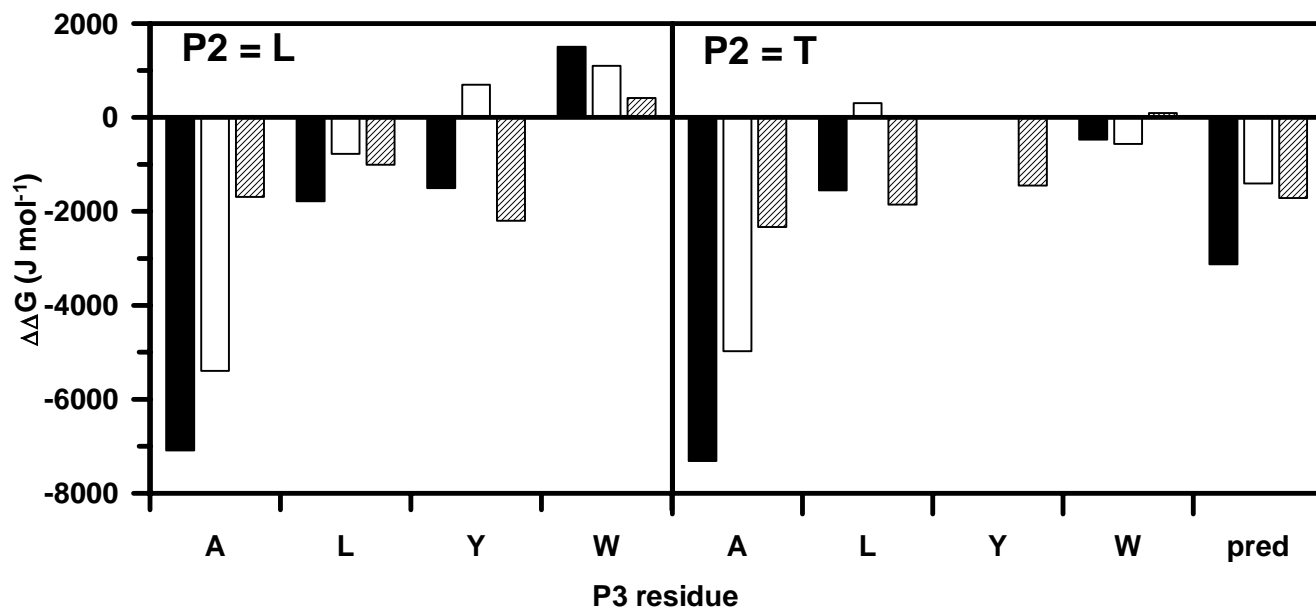


Figure 3.

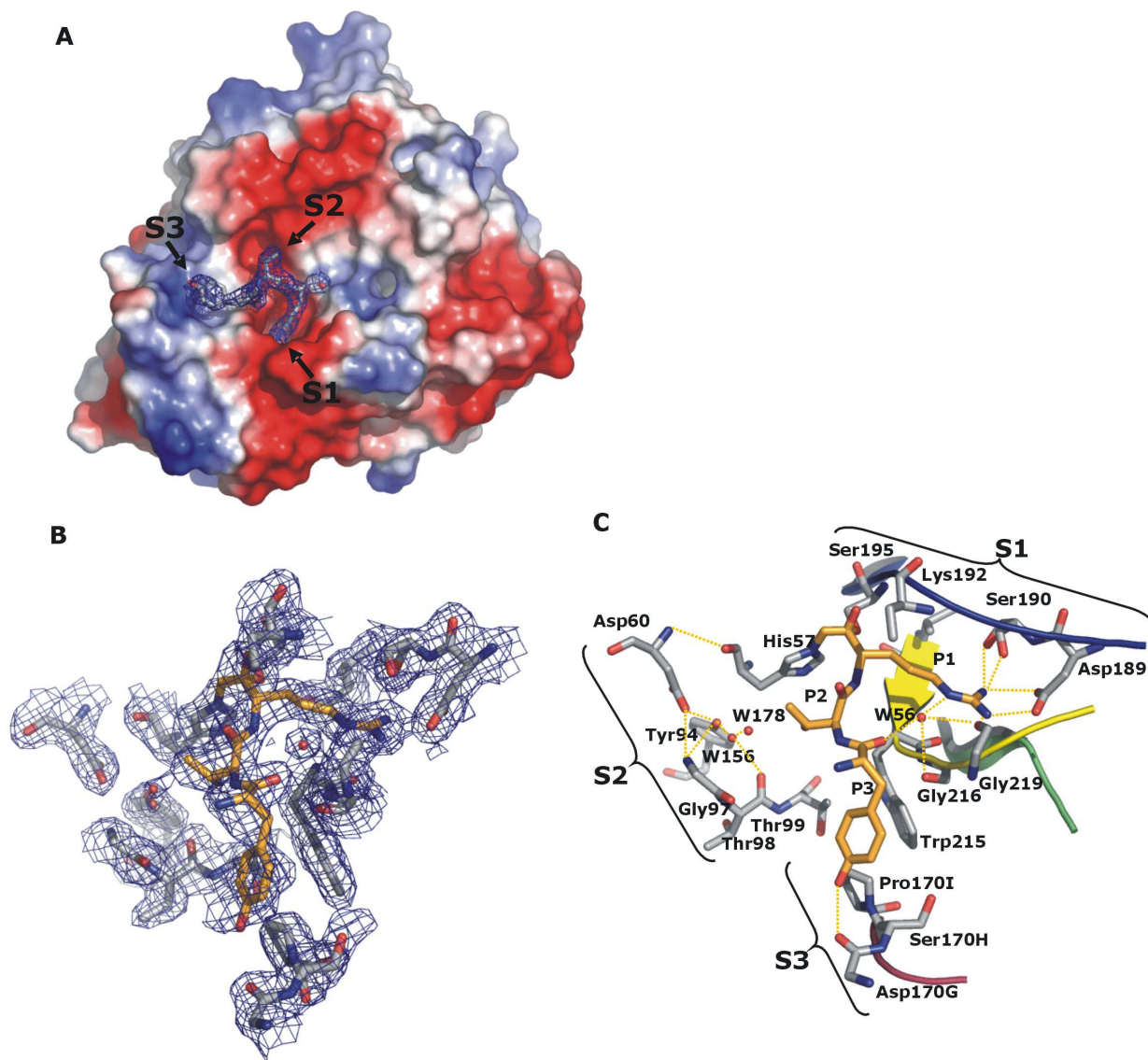


Figure 4.

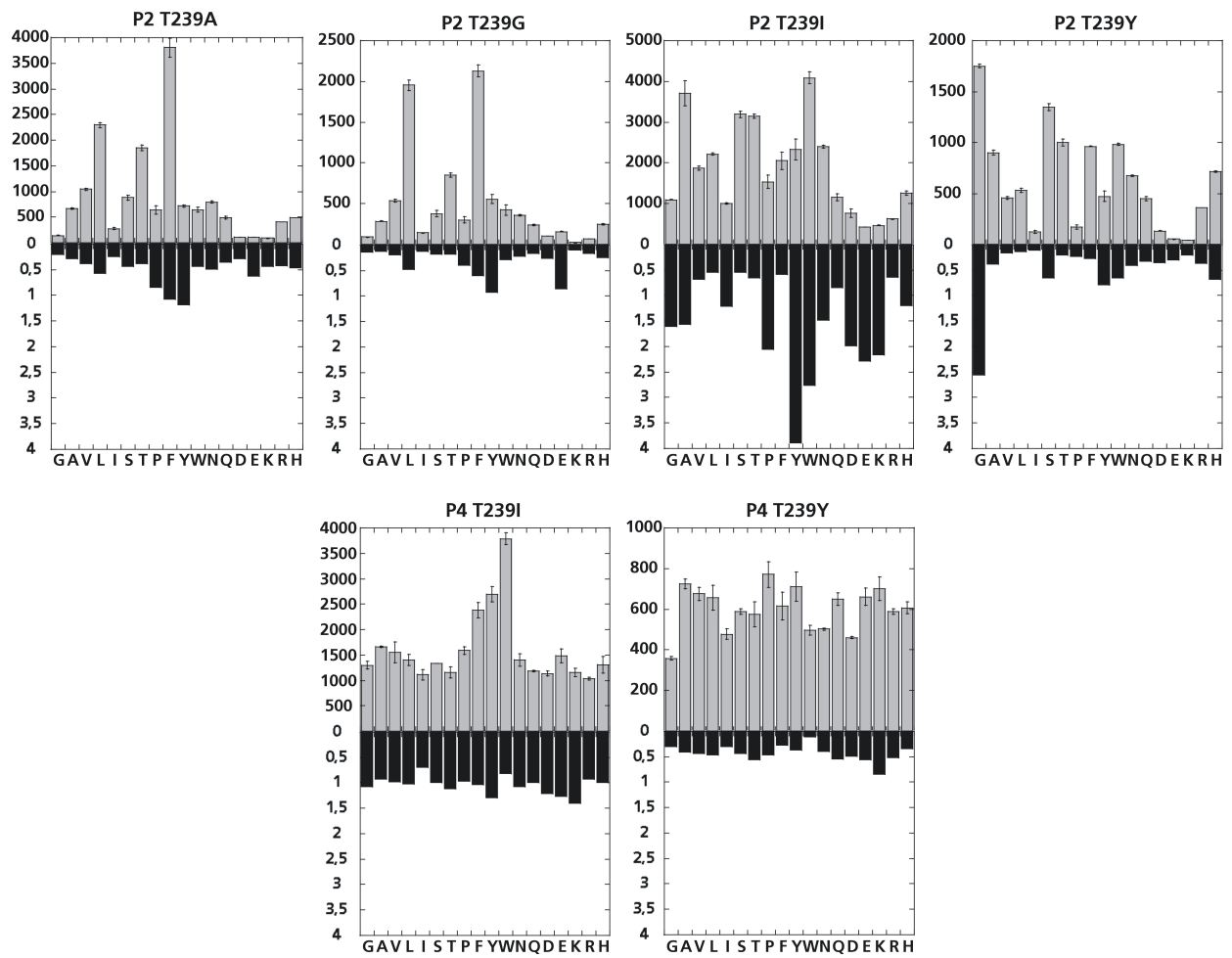


Figure 5.

